Available online at www.sciencedirect.com
SCIENCE DIRECT®
Journal of Photochemistry and Photobiology A: Chemistry 162 (2004) 89–95
Journal of Photochemistry and Photobiology A:Chemistry
www.elsevier.com/locate/jphotochem

Effects of iron species in the photocatalytic degradation of an azo dye in TiO_2 aqueous suspensions

Marta Mrowetz, Elena Selli*

Dipartimento di Chimica Fisica ed Elettrochimica, Università di Milano, Via Golgi 19, I-20133 Milan, Italy

Received 5 June 2003; received in revised form 18 June 2003; accepted 26 June 2003

Abstract

The effects of Fe(III) species on the photocatalytic degradation of azo dye Acid Red 1 (AR1) have been studied in titanium dioxide aqueous suspensions under irradiation in the 315–400 nm range. The initial increase of the photocatalytic degradation rate observed in water suspensions containing Fe(III) aquo ions (10^{-5} to 10^{-4} M) was attributed to the increased amount of dye adsorbed on the iron(III)-modified semiconductor surface. This was confirmed by the fact that iron species not adsorbed on the semiconductor, such as ferrioxalate complexes and Fe(II) species, had no kinetic effects. The mineralisation kinetic profiles obtained under simultaneous sonication further confirmed the role of AR1 adsorption. The accumulation of hydrogen peroxide during the photocatalytic degradation of the dye was completely suppressed in the presence of all iron species, mainly due to the Fenton reactions consuming H_2O_2 in the aqueous phase, although a decrease in the rate of H_2O_2 formation cannot be excluded, due to the competition between adsorbed Fe(III) species and adsorbed oxygen for photo-promoted conduction band electrons.

Keywords: Photocatalytic degradation; Titanium dioxide; Fe(III) adsorption; Acid Red 1

1. Introduction

In recent years, a great deal of interest has been devoted to the photocatalytic degradation of organic water pollutants on semiconductor particles and to the involved reaction paths. TiO_2 has been widely employed in these studies, mainly due to its outstanding photocatalytic activity and stability. The photocatalytic process leads to oxidation and finally to the overall mineralisation of a wide variety of organic pollutants, through their interaction with photo-generated holes or reactive oxygen species, such as $^{\bullet}OH$ and $^{\bullet}O_2^-$ radicals, formed on the UV-irradiated semiconductor surface [1–3]. The efficiency of the process depends on the surface properties of the semiconductor particles and, more crucially, on the mobility of the charge carriers that originate in the absorption of UV radiation, as well as on their recombination rate. Consequently, surface and/or structural modifications, such as the adsorption of positively or negatively charged species and/or doping the semiconductor by metal ions, may have a strong influence on the photocatalytic process, by altering the electron transfer pathways occurring at the water–semiconductor interface [4–7].

Dissolved metal ions are rather common in natural water and industrial wastewaters; in particular, water soluble iron species are ubiquitous [8], with concentrations ranging from 10^{-7} to 10^{-4} M. The effect of Fe(III) species on the photocatalytic degradation on TiO_2 of an azo dye has been examined in the present work by employing a radiation source, which simulates the short wavelength part of the solar spectrum. The role played by iron adsorbed on the photocatalyst and the effects of its presence in the aqueous phase both as aquo ion or in complex form have also been considered.

The investigated dye, Acid Red 1 (AR1; see Scheme 1), belongs to the largest class of dyes commonly employed in the textile and paper industry. Such dyes exhibit a very high stability under ultraviolet and visible light irradiation, the prevailing deactivation path of their electronically excited singlet state notoriously being the thermally reversible photoisomerisation around their azo double bond [9]. Moreover, they are biorecalcitrant, resistant to aerobic degradation [10] and may undergo reduction to hazardous aromatic amines under anaerobic conditions or in vivo [11,12]. The first step of their photocatalytic degradation consists in the cleavage of the azo double bond, inducing bleaching in the visible region [13–15] and the formation of reaction intermediates, which finally undergo complete mineralisation on semiconductors.

To investigate the role of Fe(III) species on the photodegradation paths prevailing both at the water–semiconduc-

* Corresponding author. Tel.: +39-02-503-14237; fax: +39-02-503-14300.
E-mail address: elena.selli@unimi.it (E. Selli).

1010-6030/$ – see front matter © 2004 Elsevier B.V. All rights reserved.
doi:10.1016/S1010-6030(03)00315-0

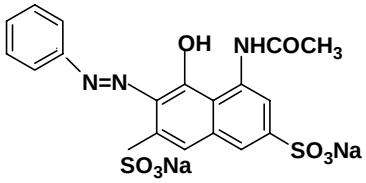

Acid Red 1 (AR1)

Scheme 1.

tor interface and in the aqueous phase, the rate of AR1 photocatalytic bleaching in the visible region was thus monitored in the present study along with the rate of overall mineralisation and with the extent of hydrogen peroxide accumulation, formed by reduction of adsorbed molecular oxygen by conduction band electrons.

2. Experimental

2.1. Materials

Acid Red 1, purchased from Aldrich, was purified by repeated crystallisation from methanol. The absence of organic contaminants was checked by NMR analysis. Titanium dioxide (Degussa P25) was employed as photocatalyst. $FeCl_3{\cdot}6H_2O$ (Sigma, purity 98%), $Fe(NO_3)_3{\cdot}9H_2O$ (Aldrich, purity >99%), $(NH_4)_3Fe(C_2O_4)_3{\cdot}3H_2O$ (Carlo Erba, purity 98%) and $FeCl_2{\cdot}4H_2O$ (Aldrich, purity >99%) were used as received. Water purified by Milli-Q water system (Millipore) was used throughout.

2.2. Apparatus

All degradation runs were carried out at $35 \pm 1\,^{\circ}C$ in a 400 ml cylindrical Pyrex closed reactor under magnetic stirring, by employing an experimental set-up analogous to that already described [16,17]. Illumination was provided by means of a 250 W iron halogenide lamp in the 315–400 nm wavelength range. The average value of its emission intensity on the reactor, periodically checked by ferrioxalate actinometry [18], was 5.8×10^{-7} einstein s^{-1} cm^{-2}. A continuous forced air circulation ensured temperature control of the whole system.

In some of the photocatalytic degradation runs, the emitting horn (12 mm diameter) of a W-385 Heat Systems Ultrasonic apparatus was inserted into the reactor through a top port [17]. This ultrasound source operated at 20 kHz with a calorimetrically determined [19] power emission of 15 W.

2.3. Procedure

Irradiated aqueous suspensions always contained 0.1 g l^{-1} of TiO_2 and a 2.5×10^{-5} M initial dye concentration. The effect of the Fe(III) addition was investigated in the 10^{-5} to 10^{-4} M concentration range; aqueous solutions containing Fe(III) species were usually prepared within 30 min before the beginning of irradiation and then kept in the dark. The pH of the AR1 suspensions decreased during the runs in the absence of iron, from an initial value of 6 to ca. 4.5, while it remained almost constant at 4.4 and 3.4 in the presence of 2.5×10^{-5} and 1.0×10^{-4} M $FeCl_3$, respectively. All runs were carried out under atmospheric conditions and constant rate stirring, as already described [16,17].

The photo-degradation of AR1 was monitored by spectrophotometric analysis at 531 nm (maximum absorption, $\varepsilon = (3.13 \pm 0.02) \times 10^4\,M^{-1}\,cm^{-1}$) by means of a Perkin-Elmer Lambda 16 apparatus [17]. The extent of mineralisation was determined through total organic carbon (TOC) analysis using a Shimadzu TOC-5000A analyser. Prior to analysis of the periodically withdrawn samples (ca. 3 ml), TiO_2 was separated from the suspensions by centrifugation at Acid Red 1 (AR1) for 30 min.

The hydrogen peroxide concentration was monitored during the photo-degradation runs by a fluorimetric analysis ($\lambda_{ex} = 316.5$ nm, $\lambda_{em} = 408.5$ nm) of the fluorescent dimer formed in the horseradish peroxidase-catalysed reaction of hydrogen peroxide with *p*-hydroxyphenylacetic acid [20,21], using a 650-10S Perkin-Elmer fluorescence spectrophotometer. H_2O_2 standard solutions employed in calibration were analysed iodometrically. This fluorimetric method was preferred to the widely employed DPD method [22], both for its higher sensitivity [23,24] and in order to avoid interferences in the spectrophotometric analysis due to the presence of AR1.

The fraction of AR1 adsorbed on the photocatalyst at 35 °C was determined both in the absence and in the presence of $FeCl_3$, by centrifugation and spectrophotometric analysis of the supernatant portion of stirred suspensions containing 0.1 g l^{-1} of TiO_2 and different concentrations of AR1. The fraction of Fe(III) adsorbed on TiO_2 at equilibrium was determined in suspensions containing 0.1 g l^{-1} of TiO_2 and an overall $FeCl_3$ concentration of 8×10^{-5} M. After centrifugation, the residual Fe(III) in the supernatant was measured by the thiocyanate method [25], after calibration under identical conditions up to $[Fe(III)] = 1.2 \times 10^{-4}$ M. The Fe(II) concentration in the aqueous phase was also determined spectrophotometrically, after complexation with *o*-phenanthroline [25].

3. Results and discussion

3.1. Adsorption and complexation equilibria involving AR1

Equilibrium adsorption of dye AR1 was measured in the presence of the same amount of titanium dioxide (0.1 g l^{-1}) employed in photocatalytic runs. The extent of adsorption was evaluated as $n_2^s = \Delta CV/W$, where n_2^s is expressed in

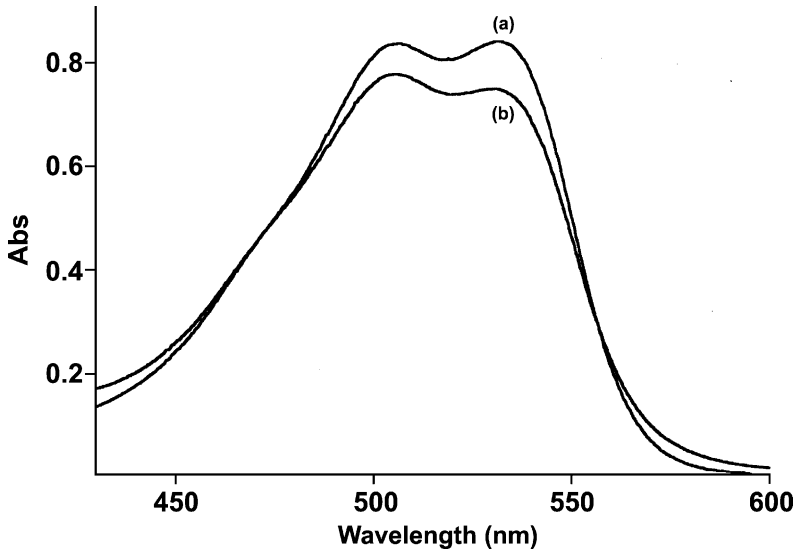

Fig. 1. Absorption spectrum of a 2.5×10^{-5} M AR1 aqueous solution before (a) and after the addition of 1×10^{-4} M $FeCl_3$ (b).

mol g^{-1}, ΔC the difference between the initial concentration and the equilibrium dye concentration in the aqueous phase, V the volume and W the weight of oxide. The heterogeneous adsorption equilibrium constant K was determined according to the procedure reported by Cunningham [26,27], by the Langmuir adsorption equation $n_2^s = n^s K C_{eq}/(1+KC_{eq})$, under conditions of a low equilibrium concentration of dye ($KC_{eq} \ll 1$). By assuming that n^s, the limiting number of dye molecules that can be adsorbed onto 1 g of TiO_2, is about 1×10^{-4} mol g^{-1}, as recently estimated from adsorption measurements of a similar azo dye on the same type of semiconductor [28], the value $K = 2 \times 10^3\ M^{-1}$ was obtained from the slope of the adsorption isotherm in the absence of Fe(III). This value is in line with the adsorption equilibrium constants on TiO_2 obtained by the same procedure for other compounds, such as substituted benzoic acids [26] and azo dyes [13,27,28]. Thus, in the absence of Fe(III) the fraction of dye adsorbed on the semiconductor at the beginning of the runs was ca. 0.02, corresponding to $n_2^s \approx 0.2$ mol g^{-1}.

The Fe(III) trivalent cation strongly interacts with TiO_2: we found that at 35 °C around 30% of Fe(III) was adsorbed on TiO_2 (0.1 g l^{-1}) at equilibrium with solutions initially containing 8×10^{-5} M $FeCl_3$. This modifies the adsorption equilibrium of AR1: the fraction of dye adsorbed on TiO_2 was found to be equal to 0.04 in the presence of 2×10^{-5} M Fe(III) (i.e. twice that on naked TiO_2) and it increased up to 0.46 in the presence of 1×10^{-4} M Fe(III). This is a consequence of the adsorption of ferric ions on TiO_2, resulting in an increased positive charge on its surface. Dye molecules, being negatively charged due to the presence of the two sulfonic groups, are more attracted by the iron(III)-modified oxide surface, as a consequence of electrostatic interaction. Moreover, also specific interaction involving the sulfonic groups of AR1, acting as monodentate ligands or as bidentate chelants through one or two oxygen atoms, respectively, are expected to be favoured by the presence of ferric ions adsorbed on the TiO_2 surface [27].

Ferric ions interact with AR1 also in the aqueous phase, as evidenced by the modification in the absorption spectrum of AR1 aqueous solutions observed after addition of Fe(III) aquo ions (Fig. 1). With the relatively low Fe(III) and AR1 concentrations employed in the present study, this effect can be attributed to the formation of a 1:1 complex in the aqueous phase between the Fe(III) species and azo dyes bearing a –OH group in the *ortho*-position with respect to the azo bond, as recently proposed in the case of an azo dye with a similar structure [29].

3.2. Kinetic effects of Fe(III) aquo ions

AR1 was found to be perfectly stable in a water solution under irradiation in the 315–400 nm wavelength range. As shown in Fig. 2, in the presence of 0.1 g l^{-1} of TiO_2, in-

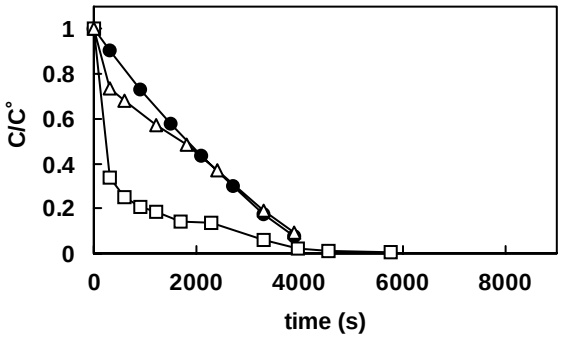

Fig. 2. Residual AR1 concentration determined by spectrophotometric analysis during the photocatalytic degradation of AR1 in the absence of $FeCl_3$ (●) and in the presence of 1×10^{-4} M (□) and 1×10^{-5} M $FeCl_3$ (△).

stead, it underwent photocatalytic degradation according to a zero-order rate law, with a rate constant of $(6.3 \pm 0.7) \times 10^{-4}\,M\,s^{-1}$. Almost complete mineralisation of AR1 could be achieved in less than 3 h, as verified by TOC analysis.

The effects of Fe(III) concentration on both AR1 photo-bleaching and photo-mineralisation rates were investigated on suspensions containing $FeCl_3$ in the 10^{-5} to 10^{-4} M concentration range. Identical kinetic runs were obtained when $Fe(NO_3)_3$ was added, instead of $FeCl_3$. This excludes any inhibiting effect of chloride anions in the photocatalytic process [30] and any relevance of $FeCl_2^+$ photolysis [31] (vide infra) in the investigated $FeCl_3$ concentration range. As shown in Fig. 2, kinetic results of AR1 photocatalytic degradation in the presence of Fe(III) aquo ions could not be interpreted according to a simple rate law, as fairly rapid bleaching was observed in the first reaction minutes, especially at a relatively high Fe(III) concentration (1×10^{-4} M), when a 66% degradation yield was attained in 5 min, followed by a slower decrease of AR1 concentration over time. For lower Fe(III) contents, the photo-degradation rate was slightly higher than on naked TiO_2 only at the beginning of irradiation.

The photocatalytic mineralisation of water suspensions (Fig. 3) proceeded at a lower rate than AR1 photo-degradation (Fig. 2), as a consequence of the accumulation of aromatic degradation intermediates formed by the azo bond cleavage [13–15]. This represents the first step of degradation, occurring when AR1 interacts with the highly reactive species produced after light absorption by the semiconductor. Such species are conduction band electrons, which combined with adsorbed dioxygen lead to $^{\bullet}O_2^-$ species, or valence band holes h^+, which readily react with adsorbed water, to give $^{\bullet}OH$ radicals [1–3]. Photo-degradation may also occur through a photosensitised route when, as is the case of azo dyes, photo-degradation substrates are able to absorb light directly and to inject electrons from their excited state into the conduction band of the semiconductor [13,32]. The subsequently formed oxidising species, as well as molecular oxygen, can then attack the so formed dye radical cation, inducing its degradation. This

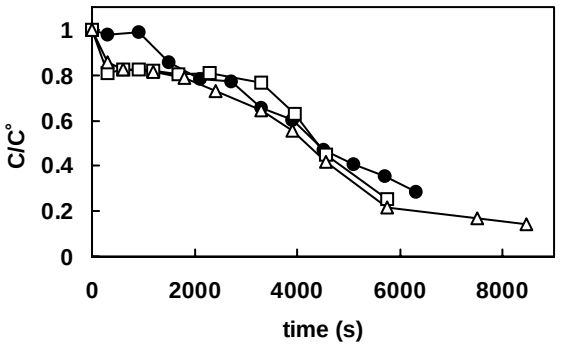

Fig. 3. Residual TOC content during the photocatalytic degradation of AR1 in the absence of $FeCl_3$ (●) and in the presence of 1×10^{-4} M (□) and 1×10^{-5} M $FeCl_3$ (△).

reaction path, depending on the extent of dye adsorption on TiO_2 particles, may have more or less importance. In the present case, however, it should not represent the prevailing reaction route, as AR1 absorbs moderately in the range of irradiation wavelengths employed here.

While in the absence of iron the mineralisation rate was almost constant (Fig. 3), kinetic runs carried out in the presence of Fe(III) always exhibit an initial decrease of organic carbon content in the aqueous phase, followed by a sort of plateau, which lasts longer when increasing the overall Fe(III) amount, and a subsequent further mineralisation step, up to very low ($<1\,mg\,l^{-1}$) TOC contents. Both AR1 concentration and mineralisation versus time profiles were not affected by simultaneous modifications of the adsorption equilibria involving Fe(III) and AR1, as identical kinetic runs were obtained by starting irradiation after a different equilibration time ($\geq$30 min) of the TiO_2–Fe(III)–AR1 aqueous system, thus confirming that adsorption equilibria involving such dyes are quite fast [33].

The effects of Fe(III) species both in the aqueous phase and adsorbed onto the photocatalyst should be taken into account when discussing the observed kinetic behaviour. $Fe(OH)^{2+}$, the monomeric Fe(III)-hydroxy species predominant in aqueous solutions in the pH range 2.5–5.5 [34], is the most photoactive Fe(III) species in the 300–400 nm range [34–37], its photolysis leading to the formation of $^{\bullet}OH$ radicals in aqueous systems:

$$Fe(OH)^{2+} + h\nu \rightarrow Fe^{2+} + {}^{\bullet}OH \quad (1)$$

Absorption of light in the solvent/ligand to metal charge transfer band of this complex causes a partial charge transfer from a ligand-centred orbital to a metal-centred orbital. Other Fe(III) complexes, such as $Fe(OH)_2^+$ prevailing at pH >5.5, are less photo-reactive. Fe^{2+} does not absorb light above 300 nm and therefore it is not expected to undergo photolysis under the adopted experimental conditions.

To discriminate between photo-induced effects occurring at the water–semiconductor interface or in the aqueous phase, the effects of $FeCl_3$ photoactivity on AR1 photo-degradation were investigated in the absence of TiO_2. Results reported in Fig. 4 are indicative of an almost negligible (ca. 1%) AR1 photo-degradation occurring in the 2×10^{-5} M $FeCl_3$ solution; a decrease of AR1 concentration was observed, instead, under irradiation in the presence of 10^{-4} M $FeCl_3$, up to ca. 30% AR1 photo-degradation. This reaction proceeded in the aqueous phase up to the complete transformation of Fe(III) species into Fe(II) species, as also evidenced in the aqueous phase degradation of a similar azo dye induced by UV/Fe(III)-generated hydroxyl radicals [37]. Moreover, photo-induced iron reduction could occur in the system under study also as a result of a ligand to metal charge transfer in the above-mentioned Fe(III)–AR1 complex, leading to the formation of the dye radical cation, as recently hypothesised for a similar system on the basis of laser photolysis studies [29]. Regardless, the initial accelerating effect observed in the presence of Fe(III) species

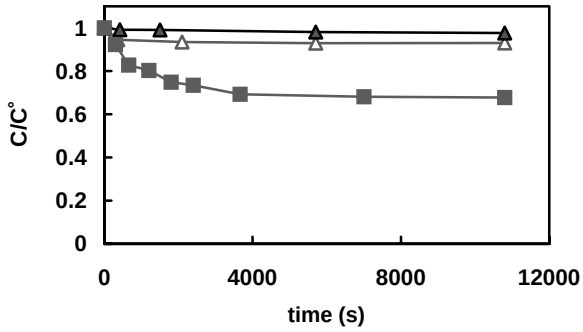

Fig. 4. Residual AR1 concentration determined by spectrophotometric analysis during the aqueous phase photo-induced degradation of AR1 in the presence of 2×10^{-5} M (▲) or 1×10^{-4} M $FeCl_3$ (■) and 2×10^{-5} M $(NH_4)_3Fe(C_2O_4)_3$ (△).

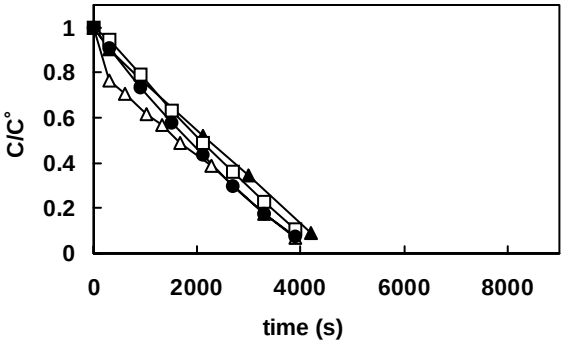

Fig. 5. Residual AR1 concentration determined by spectrophotometric analysis during the photocatalytic degradation of AR1 in the absence of iron (●) and in the presence of 2×10^{-5} M $(NH_4)_3Fe(C_2O_4)_3$ (□), $FeCl_2$ (▲) and $FeCl_3$ (△).

on the overall AR1 photocatalytic degradation rate (Fig. 2) can be attributed only in part to homogeneous phase reactions: in irradiated aqueous suspensions such an effect is much more evident than one may expect from aqueous phase photo-degradation tests in the presence of the same Fe(III) amount (Fig. 4), also taking into account that in water suspensions Fe(III) aquo ions can absorb only a very small fraction of the incident radiation.

Thus, interface phenomena play a role in the observed increase of the AR1 photo-degradation rate. The increase of dye adsorption on TiO_2 observed in the presence of Fe(III) species is expected to have beneficial effects on the rate of photoredox processes occurring at the water–semiconductor interface, as the oxidising species photo-generated on the semiconductor do not migrate far from the photo-generated active centres: the photocatalytic degradation process occurs at the surface or within a few monolayers around the photocatalytic particles [38]. Controversial effects of Fe(III) adsorption on TiO_2 have been reported: for instance, iron species adsorbed on the semiconductor were found to increase the recombination rate of electrons and holes [6], thus inhibiting interface photo-induced processes, but were also found to have a catalytic function for the oxidation of water on photo-irradiated TiO_2 [39]. The simplest explanation of the present kinetic results, obtained at relatively a low Fe(III) concentration, is that the increased AR1 adsorption on the Fe(III)-modified semiconductor surface should prevail in determining the observed increase of the overall degradation rate.

TOC monitoring of kinetic runs (Fig. 3) show that the active species photo-generated on the semiconductor, as well as the hydroxyl radicals produced by reaction (1), whose concentration is expected to increase with an increasing Fe(III) amount, preferentially attack the azo double bond of the dye rather than the aromatic rings, leading to a low mineralisation efficiency of the degradation intermediates: a marked difference can be noticed between the high initial AR1 photo-degradation rate (Fig. 2) and the almost zero mineralisation rate in the plateau of Fig. 3, corresponding to the transformation of AR1 into degradation intermediates, without any decrease in the overall TOC content. Also, differences in the adsorption capacity on iron-modified TiO_2 between AR1, bearing two sulfonic groups undergoing specific interaction with the oxide surface [27], and the degradation intermediates, which may have undergone desulfonation [33], may contribute to the establishment of the plateau in the TOC versus time profiles of Fig. 3.

3.3. Effect of Fe(III) complexes and of Fe(II) species

The importance of AR1 adsorption on its photo-degradation rate was confirmed by kinetic runs carried out after the addition of $(NH_4)_3Fe(C_2O_4)_3$ and $FeCl_2$ (Fig. 5). First of all, the abrupt initial decrease in AR1 concentration observed in the presence of $FeCl_3$ and $Fe(NO_3)_3$ was not revealed in this case. Indeed, Fe(II) ions exhibit a lower affinity for the oxide surface than Fe(III) cations [39], while ferrioxalate anions do not significantly adsorb on the semiconductor surface, but prevalently remain in the aqueous phase as stable $[Fe(C_2O_4)_2]^-$ and $[Fe(C_2O_4)_3]^{3-}$ complexes [40,41].

Photocatalytic AR1 degradation (Fig. 5) exhibits a typical zero-order kinetic behaviour in the presence of these iron species, at a slightly lower rate than that determined in the absence of iron ions, the measured rate constant being $k = (5.4 \pm 0.3) \times 10^{-4}$ and $(5.7 \pm 0.2) \times 10^{-4}$ M s^{-1} in the presence of Fe(II) and ferrioxalate, respectively. Also the mineralisation versus time profile obtained by TOC analysis in the presence of ferrioxalate and ferrous ions appear to almost coincide with that obtained in the absence of iron and reported in Fig. 3, with AR1 mineralisation occurring at an almost constant rate (no plateau regions). Thus, the kinetic behaviour appears scarcely affected by both aqueous phase Fe(III) oxalate species and Fe(II) ions, exhibiting no adsorption on TiO_2, although ferrioxalate anions are known to be photoactive [41,42]. Indeed, as shown in Fig. 4, AR1 was found to undergo photo-degradation in aqueous solutions containing 2×10^{-5} M ferrioxalate, up to a degree slightly higher than that achieved in the presence of the same amount

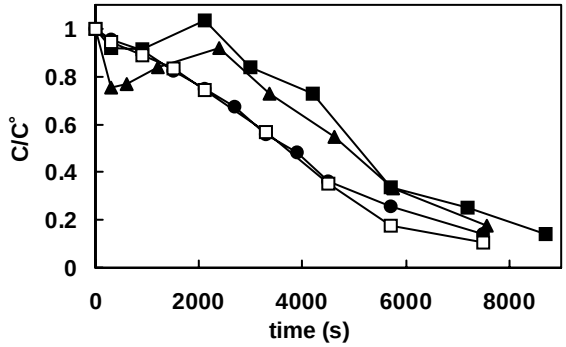

Fig. 6. Residual TOC content during the sonophotocatalytic degradation of AR1 in the absence of iron (●) and in the presence of 2×10^{-5} M $(NH_4)_3Fe(C_2O_4)_3$ (□) and 1×10^{-4} M (▲) or 2×10^{-5} M $FeCl_3$ (■).

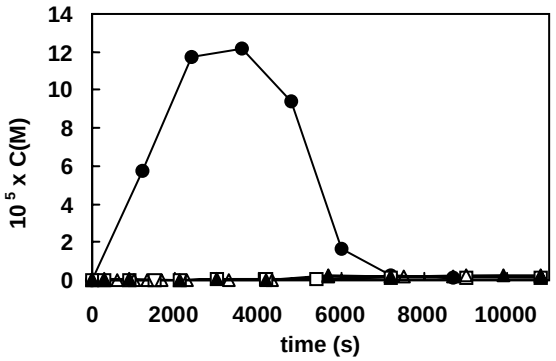

Fig. 7. H_2O_2 concentration during the photocatalytic degradation of AR1 in the absence of iron (●) and in the presence of 2×10^{-5} M $(NH_4)_3Fe(C_2O_4)_3$ (□), $FeCl_3$ (△) and $FeCl_2$ (▲).

of Fe(III) aquo ions. However, no increase in the overall AR1 photo-degradation rate was observed in TiO_2 suspensions containing ferrioxalate anions, due to the fact that the latter should absorb a negligible fraction of incident light in AR1 suspensions. Thus, the accelerating effect observed in the presence of adsorbed Fe(III) is mainly attributable to an increased AR1 adsorption.

3.4. Effect of sonication

Further evidence of the role of Fe(III) adsorption was obtained from AR1 photocatalytic degradation runs carried out under simultaneous sonication, i.e. under the so-called sonophotocatalytic conditions [17,43]. Ultrasound promotes the desorption of species adsorbed at the liquid–solid interface. Simultaneous sonication in the presence of iron species was found to have no effect on the rate of AR1 photo-bleaching. The results of TOC monitoring of sonophotocatalytic runs carried out in the presence of different iron species are shown in Fig. 6. In the presence of $FeCl_3$, the TOC content in the aqueous phase first decreased, then increased up to values very close to the initial amount. This behaviour was more evident in the cases of higher Fe(III) adsorption (higher $FeCl_3$ concentration). Subsequently, the mineralisation proceeded at almost the same rate as in the other runs, while total mineralisation was of course achieved later. Both effects are a consequence of the fact that ultrasound promotes the desorption of both AR1 and degradation intermediates weakly adsorbed on TiO_2, thus decreasing the rate of the photocatalytic mineralisation process, occurring at the water–semiconductor interface. In fact, no differences in the TOC monitoring profile were observed between the photocatalytic and the sonophotocatalytic runs carried out in the presence of either Fe(II) or ferrioxalate species (Fig. 6).

3.5. H_2O_2 evolution

Finally, the concentration of hydrogen peroxide was also determined during the photo-degradation runs carried out in the presence of different iron species. Hydrogen peroxide was demonstrated to form exclusively through the reduction of molecular oxygen by conduction band electrons [44]. H_2O_2 development under irradiation was reported also from ferrioxalate complexes [41].

As shown in Fig. 7, hydrogen peroxide was found to accumulate from the beginning of irradiation during AR1 photocatalytic degradation on naked TiO_2; its concentration was found to increase over time, attaining a maximum value ($[H_2O_2]_{max} = 1.2 \times 10^{-4}$ M) after 60 min irradiation, followed by a progressive decrease consequent to the progressively decreasing concentration of organic species undergoing oxidation. Indeed, in the absence of species able to rapidly react with the photo-generated holes, the electron–hole recombination reaction becomes faster than molecular oxygen reduction. In the presence of iron species, instead, the H_2O_2 concentration was much lower, always remaining below the detection limit of 2.5×10^{-6} M, up to the complete disappearance of the dye (Fig. 7).

The lower concentration of hydrogen peroxide in the presence of Fe(III) might be due both to a lower rate of formation of such an intermediate and to an increase of its decomposition rate through the following aqueous phase Fenton reactions [45]:

$$Fe(III) + H_2O_2 \rightarrow Fe(II) + {}^{\bullet}OOH + H^+ \quad (2)$$

$$Fe(II) + H_2O_2 + H^+ \rightarrow Fe(III) + H_2O + {}^{\bullet}OH \quad (3)$$

The presence of Fe(III) adsorbed on the photocatalyst, acting as an oxidising species able to combine with conduction band electrons in competition with molecular oxygen [7], may contribute in decreasing the rate of H_2O_2 formation. This hypothesis is confirmed by the fact that at the end of the runs Fe(III) was not detected in the aqueous phase, but was quantitatively converted into Fe(II). Fe(III) reduction by conduction band electrons is thermodynamically possible, as the redox potential of the Fe^{3+}/Fe^{2+} couple is $E^{\circ}(Fe^{3+}/Fe^{2+}) = 0.771$ V (NHE), while the potential of the TiO_2 conduction band is $E_{cb} = -0.5$ V (NHE) at pH 1 [1,7]. However, as hydrogen peroxide did not accumulate

in the aqueous phase even in the presence of Fe(II), reactions (2) and (3) should play a major role in maintaining H_2O_2 concentration below the detection limit: in fact, hydrogen peroxide formation is not expected to be inhibited in the presence of Fe(II) species.

References

[1] M.R. Hoffmann, S.T. Martin, W. Choi, D.W. Bahnemann, Chem. Rev. 95 (1995) 69.
[2] A.L. Linsebigler, L. Guangquan, J.T. Yates Jr., Chem. Rev. 95 (1995) 735.
[3] D. Bahnemann, J. Cunningham, M.A. Fox, E. Pelizzetti, P. Pichat, N. Serpone, in: G.R. Helz, R.G. Zepp, D.G. Crosby (Eds.), Aquatic and Surface Photochemistry, Lewis, Boca Raton, FL, 1994, p. 261.
[4] A. Sclafani, L. Palmisano, E. Davì, J. Photochem. Photobiol. A: Chem. 56 (1991) 113.
[5] W. Choi, A. Termin, M.R. Hoffmann, J. Phys. Chem. 98 (1994) 13669.
[6] S. Ikeda, N. Sugiyama, B. Pal, G. Marcì, L. Palmisano, H. Noguchi, K. Uosaki, B. Ohtani, Phys. Chem. Chem. Phys. 3 (2001) 267.
[7] C. Chen, X. Li, W. Ma, J. Zhao, H. Hidaka, N. Serpone, J. Phys. Chem. B 106 (2002) 318.
[8] T.E. Graedel, M.L. Mandich, C.J. Weschler, J. Geophys. Res. 91 (1986) 5205, and references therein.
[9] H. Zollinger, Color Chemistry—Synthesis, Properties and Application of Organic Dyes and Pigments, VCH Publishers, New York, 1987.
[10] U. Pagga, D. Brown, Chemosphere 15 (1986) 479.
[11] G.M. Shaul, T.J. Holdsworth, C.R. Dempsey, K.A. Dostal, Chemosphere 22 (1991) 107.
[12] F. Rafii, W. Franklin, C.E. Cerniglia, Appl. Environ. Microbiol. 56 (1990) 2146.
[13] K. Vinodgopal, D.E. Wynkoop, P.V. Kamat, Environ. Sci. Technol. 30 (1996) 1660.
[14] J. Bandara, J.A. Mielczarski, J. Kiwi, Langmuir 15 (1999) 7680.
[15] C. Bauer, P. Jacques, A. Kalt, J. Photochem. Photobiol. A: Chem. 140 (2001) 87.
[16] V. Ragaini, E. Selli, C.L. Bianchi, C. Pirola, Ultrason. Sonochem. 8 (2001) 251.
[17] E. Selli, Phys. Chem. Chem. Phys. 4 (2002) 6123.
[18] C.G. Hatchard, C.A. Parker, Proc. R. Soc. London A 235 (1956) 518.
[19] T.J. Mason, Practical Sonochemistry, Ellis Horwood, Chichester, UK, 1991, p. 45.
[20] G.G. Guilbault, P.J. Brignac Jr., M. Juneau, Anal. Chem. 40 (1968) 1256.
[21] C. Kormann, D.W. Bahnemann, M.R. Hoffmann, Environ. Sci. Technol. 22 (1988) 798.
[22] H. Bader, V. Sturzenegger, J. Hoigné, Water Res. 22 (1988) 1109.
[23] R. Schick, I. Strasser, H.-H. Stabel, Water Res. 31 (1997) 1371.
[24] K. Kosaka, H. Yamada, S. Matsui, S. Echigo, K. Shishida, Environ. Sci. Technol. 32 (1998) 3821.
[25] E.B. Sandell, Colorimetric Determination of Traces of Metals, Interscience, New York, 1950, pp. 362, 375.
[26] J. Cunningham, G. Al-Sayyed, S. Srijaranai, in: G.R. Helz, R.G. Zepp, D.G. Crosby (Eds.), Aquatic and Surface Photochemistry, Lewis, Boca Raton, FL, 1994, p. 317.
[27] J. Bandara, J.A. Mielczarski, J. Kiwi, Langmuir 15 (1999) 7670.
[28] Y. Xu, C.H. Langford, Langmuir 17 (2001) 897.
[29] V. Nadtochenko, J. Kiwi, J. Chem. Soc., Faraday Trans. 93 (1997) 2373.
[30] M. Abdullah, J.K.C. Low, R.W. Matthews, J. Phys. Chem. 94 (1990) 6820.
[31] V.A. Nadtochenko, J. Kiwi, Inorg. Chem. 37 (1998) 5233.
[32] T. Wu, G. Liu, J. Zhao, H. Hidaka, N. Serpone, J. Phys. Chem. B 103 (1999) 4862.
[33] K. Tanaka, K. Padermpole, T. Hisanaga, Water Res. 34 (2000) 327.
[34] B.C. Faust, J. Hoigné, Atmos. Environ. 24A (1990) 79.
[35] H.-J. Benkelberg, P. Warneck, J. Phys. Chem. 99 (1995) 5214.
[36] P. Mazellier, M. Sarakha, M. Bolte, New J. Chem. 23 (1999) 133.
[37] Y. Xu, H. Lu, J. Photochem. Photobiol. A: Chem. 136 (2000) 73.
[38] C. Minero, F. Catozzo, E. Pelizzetti, Langmuir 8 (1992) 481.
[39] T. Ohno, D. Haga, K. Fujihara, K. Kaizaki, M. Matsumura, J. Phys. Chem. B 101 (1997) 6415.
[40] D.A. Skoog, D.M. West, F.J. Holler, Fundamentals of Analytical Chemistry, sixth ed., Saunders, Philadelphia, 1992.
[41] Y. Zuo, J. Hoigné, Environ. Sci. Technol. 26 (1992) 1014.
[42] B.C. Faust, R.G. Zepp, Environ. Sci. Technol. 27 (1993) 2517.
[43] M. Mrowetz, C. Pirola, E. Selli, Ultrason. Sonochem. 10 (2003) 247.
[44] A.J. Hoffman, E.R. Carraway, M.R. Hoffmann, Environ. Sci. Technol. 28 (1994) 776.
[45] C. Walling, Acc. Chem. Res. 8 (1975) 125.